

Modeling Microtopographic Effects in Watershed-scale Integrated Surface/Subsurface Models

Abstract

In permafrost-affected regions, subsurface is mainly characterized by ice-wedge polygons and manifests a patterned polygonal ground. The role of patterned polygonal ground and associated fine-scale microtopography (spatial heterogeneities at a scale smaller than the size of polygons) in controlling surface/subsurface thermal hydrology is critical but well-understood. Fine-scale simulations are required to capture microtopographic influences on flow. Standalone fine-scale surface hydrology simulations are feasible with modern computing tools. However, highly resolved integrated surface/subsurface thermal hydrology simulations are not tractable at watershed scale and requires proper modeling. To capture the effects of microtopographic features (such as depressions, obstructions etc.) in coarsened model, we present a subgrid model parameterized by small-scale spatial heterogeneities. The subgrid model alters the water storage and flow terms in the existing governing equations. We demonstrate how a few parameters extracted from the available fine-scale information can be utilized to account for microtopographic effects in coarsened watershed-scale integrated models. Simulations were carried out and numerical results of the subgrid model were compared both to those generated with no subgrid model and to fine-scale results of seven ice-wedge polygons. Our findings confirm that the subgrid model improves the shape of the hydrographs and the to-

tal water content in the system, and that the results are very close to the corresponding fine-scale simulations. Watershed-scale fully integrated surface/subsurface simulations with the subgrid model show that the surface depressions increase infiltration and reduce runoff, thereby highlighting the importance of microtopographic effects on the watershed-scale hydrology.

Keywords: Subgrid model, Polygonal tundra, Microtopography, Watershed, Integrated Surface/Subsurface

1. Introduction

A large amount of frozen organic carbon is stored in permafrost-affected soils of the Northern Hemisphere [1, 2]. The ground in the Arctic regions is temperature-sensitive and under potential risk of carbon release to the atmosphere in a changing climate [3]. Arctic landscapes are dominated by polygonal patterned (interconnected polygons) ground. The formation of polygonal landscapes in permafrost-affected regions is a consequence of recurring cracks-compression process over hundreds of thousands of years. During winter, vertical fractures are formed due to ground contraction, the water from the snowmelt in the following summer penetrates those cracks and refreezes. In the following winter, the reexpansion of the ice in the cracks compresses the soil horizontally. The recurring crack-compression process over long period of time develops wedges of ice and finally a polygonal landscape is formed [4, 5, 6, 7]. Figure 1 displays a polygonal tundra, a field site of the U.S. Department of Energy’s Next Generation Ecosystem Experiments (NGEE) Arctic project located within the Barrow Environmental Observatory (BEO) [8]. Several types of polygons are formed due to permafrost degradation. Typically, the polygons are classified as low-centered

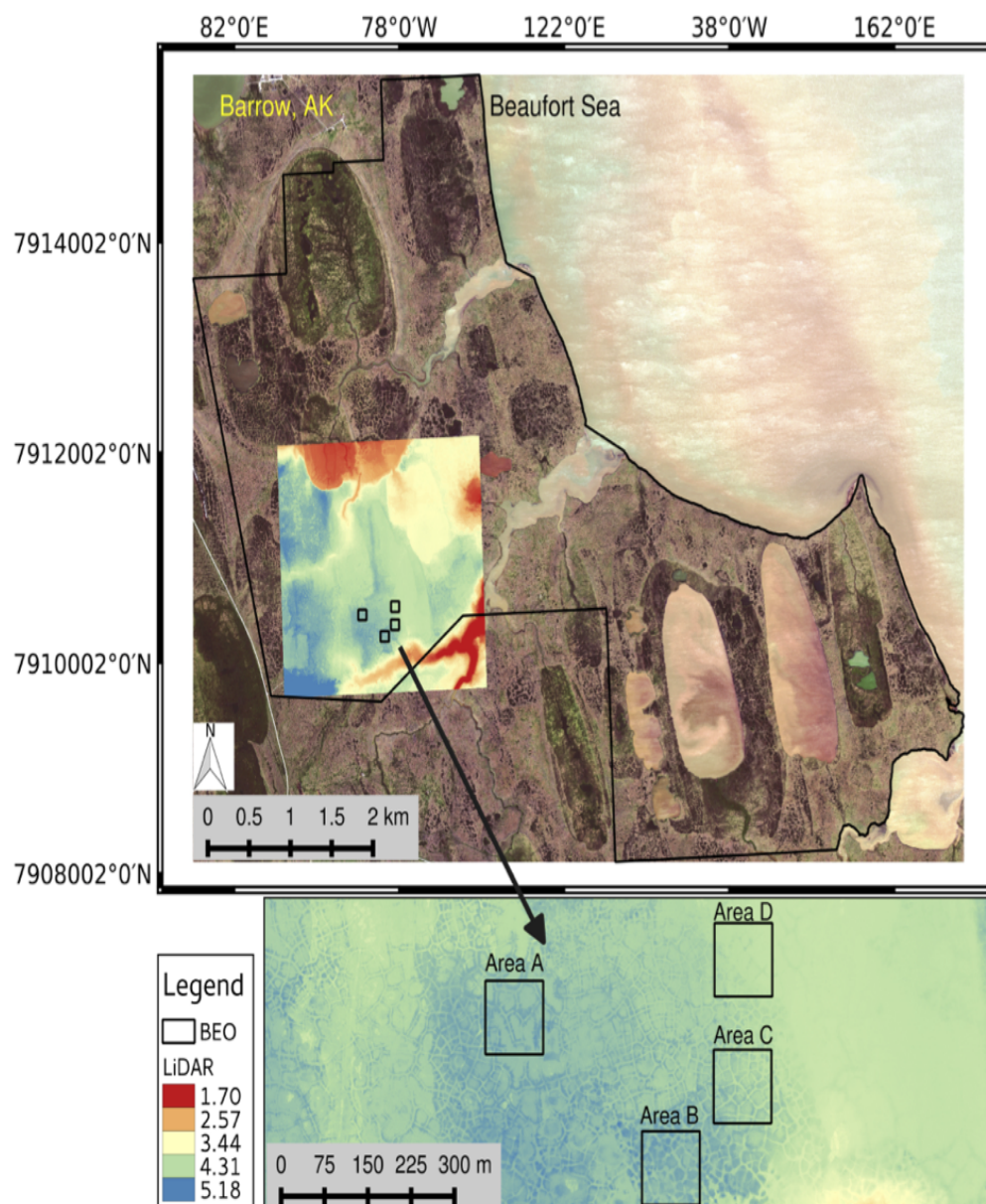


Figure 1: NGEE-Arctic field sites at BEO [8].

20 polygon (LCP) and high-centered polygon (HCP) based on surface microtopography. The LCP has a raised rim and central depression, thereby holds ponded water in the center during the summer that can only be available for infiltration and evaporation. The HCP has elevated center that slopes downward to trough and enhances runoff, thus the center may remain mostly dry. Thawing of ice-wedges causes the raised rims of LCP to subside that leads
25 to the formation of HCP [9]. The loss of depression storage in the LCP has the ability to connect the disconnected troughs, thus transforms a poorly drained tundra to a well-established drainage network. Those changes will potentially alter the entire ecosystem and will bring substantial hydrological changes (e.g., surface/subsurface interactions, distribution of surface water,
30 discharge rate etc.) [10, 3, 11, 12].

To better understand the interactions between surface and subsurface, surface runoff and discharge rate, it is important to gain insight into the role of heterogeneous spatial structure of the ground surface. It is well understood that spatial heterogeneities in the surface microtopography (un-
35 evenness at small scale) serve a critical role in surface water retention, surface/subsurface interactions, delay runoff, and thereby significantly affects the shape of hydrographs [13][**References**]. In general, an accurate flow representation is achieved at fine-scale (a scale of centimeters) and fortunately with the availability of sophisticated simulation tools, standalone
40 highly resolved surface-flow simulations are easily tractable. However, fully integrated surface/subsurface thermal hydrology simulations with highly resolved computational grid are not tractable at watershed scale. That said, if the microtopographic effects are ignored in the integrated models, the processes representing flow will not be completely accurate. The idea to
45 incorporate fine-scale flow behavior in the watershed-scale integrated mod-

els motivates the use of subgrid representation. A subgrid model is build on the information gained from highly resolved surface topographic data: the depressions and obstructions. Depressions are disconnected low points in the topography (surface pits) that retain water that is available only for infiltration or/and evaporation. Obstructions are objects exit above the depressions that interrupt and slow the flow, but do not completely block it. To incorporate the microtopographic features in the governing equations, the accumulation term is altered to account for depressions, and a modified flow law is used to introduce obstructions; more details are provided in the subsequent sections. It is worth to point out, that we intend to use the subgrid parametrization with a mixed-dimensional model reported here [14], where the subsurface is discretized as independent columns and coupled through a surface flow system. In this work, the subgrid parameterization is applied to the lateral flow part only, which is the surface system. This is one aspect of incorporating the microtopographic effects in watershed-scale integrated models, however, in general, both the surface and subsurface require a subgrid model. In this work, we are testing a hypothesis that the effects of microtopography can be captured in coarsened models through the use of a subgrid model. We evaluate one possible form of that model, and explore how parameters can be deduced from the available information.

Pertinent to the literature, integrated surface/subsurface modeling has received considerable attention from researchers across the world; see, for example, [15, 16, 17] and references therein. Here we focus only on the subgrid modeling approach. Though the concept of microtopographic features and their implications on the flow and discharge is not new, but has not been fully addressed and understood from modeling perspective. In the mid-1950s, the significance of the surface microtopographic features were

described in [18]. A one-dimensional simulations to study the effects of spatially varying surface roughness on flow hydrographs is presented in [13].
75 Panday and Huyakorn (2004) presented an integrated surface/subsurface flow model with subgrid representation through the surface depressions and obstructions by modifying the overland flow governing equation. **INCOMPLETE!!**

The rest of the paper is organized as follows. Section 2 introduces the
80 derivation of the governing equations of the subgrid model. A short description, for a quick reference, of the Advanced Terrestrial Simulator (ATS) and the Arcos multiphysics management framework, within which we implemented our subgrid model, is presented in Section 3. In Section 4 we compare the numerical results of our subgrid model with no subgrid model
85 and fine-scale results to illustrate the accuracy of our subgrid model for capturing fine-scale microtopographic features. Finally, in Section 5, we offer closing remarks and future research inline with thaw-induced subsidence.

2. Subgrid Model

This section describes the derivation of the subgrid model. The subgrid model alters the accumulation term and the flow law. For example, the ponded depth in the accumulation term is typically replaced with a volumetric depth, the ponded depth that would occur if the surface were flat. Specifically, we make the substitution in the accumulation term, where is ponded depth. The volumetric head may be calculated on geometric arguments. Specifically, if the microtopographic elevation field on an ice-wedge polygon (IWP) is $Z_*(x, y)$, the the volumetric depth is

$$\Phi(\delta) = \frac{1}{A} \iint (\delta + Z_0 - Z_*(x, y)) H(\delta + Z_0 - Z_*(x, y)) dx dy. \quad (1)$$

Where the integration is over the surface of the IWP, A is the area of the
90 IWP, Z_0 is the minimum elevation in the IWP, and H is the Heaviside
function. This could be computed from the microtopography and stored as
a lookup table. Or, we could employ a simpler parameterization. To that
end, we consider parameterizing the microtopography with two parameters:
(1) the elevation range spanned by the subgrid microtopography δ_{\max} , and
95 (2) the specific excluded volume δ_{ex} , which is the soil volume per unit bulk
area. Then, we approximate the volumetric depth as

$$\Phi(\delta) = \begin{cases} (2\delta_{\max} - 3\delta_{\text{ex}}) \left(\frac{\delta}{\delta_{\max}}\right)^2 + (2\delta_{\text{ex}} - \delta_{\max}) \left(\frac{\delta}{\delta_{\max}}\right)^3 & \text{if } 0 \leq \delta \leq \delta_{\max}, \\ \delta - \delta_{\text{ex}} & \text{if } \delta > \delta_{\max}. \end{cases} \quad (2)$$

The volumetric depth calculated from the approximation (Equation 2) is
compared (curve) with the direct calculation (Equation 1 (dots)) for four
ice-wedge polygon in Figure 2 and representative of other polygons. Also,
shown is the volumetric depth in the absence of microtopography, which is
linear with slope unity. Equation 1 is a very good approximation. Microto-
pographic effects on the flow law are not as straightforward to incorporate
as the volumetric head $\Phi(\delta)$. In particular, we should make the distinction
between depressions and obstructions (Panday and Huyakorn, 2004). De-
pressions are disconnected low points in the topography. The ponded depth
must rise above the level of those depressions before any flow can happen.
Obstructions exist above the depressions and interrupt and slow the flow,
but do not block it completely. To model the effects of obstructions and
depressions, we propose the following modification to the flow law

$$U = -\Theta(\delta) \frac{(\delta - \delta_d)^{2/3}}{n_{\text{mann}}(\|\nabla Z\| + \epsilon)^{1/2}} \quad (3)$$

where δ_d is the depression depth, and $\Theta(\delta) \in [0, 1]$ is a fractional conductance which account for flow reduction by obstructions. polygons-finescale

To calculate δ_d from the microtopography, we now propose an approach
 100 based on site percolation. Specifically, we fill the lowest elevation surface cells until the cluster of inundated cells spans the IWP. This is the percolation threshold. The water height at the percolation threshold defines the δ_d . Figure 3 shows the spanning cluster at the percolation threshold for the IWP C40 shown in Figure 4. The depression depth calculated this way is 4.1
 105 cm for this IWP. It is reasonable to assume that the fractional conductance is well approximated by the fractional cross section available to flow, which can be estimated as the ratio of volumetric depth to ponded depth.

$$\Theta(\delta_d) \approx \frac{(\Phi(\delta) - \Phi(\delta_d))}{\delta} H(\delta - \delta_d) \quad (4)$$

Where H is the Heaviside function. The numerator is the flowing cross sectional area. Note the velocity is multiplied by ponded depth to get a
 110 flux, so the molar flux appearing in the conservation equations becomes

$$\eta_l \delta U = -\eta_l (\Phi(\delta) - \Phi(\delta_d)) H(\delta - \delta_d) \Theta(\delta) \frac{(\delta - \delta_d)^{2/3}}{n_{\text{mann}}(\|\nabla Z\| + \epsilon)^{1/2}} \nabla(Z + \delta) \quad (5)$$

In summary, we hypothesize that the microtopographic effects on surface flow can be captured with a simple approximation with three parameters that can be computed from the microtopography:

- 115 • Subgrid relief $\delta_{\text{max}} = Z_{*,\text{max}} - Z_{*,\text{min}}$, where $Z_{*,\text{max}}$ and $Z_{*,\text{min}}$ are the maximum and minimum elevation in the microtopography.

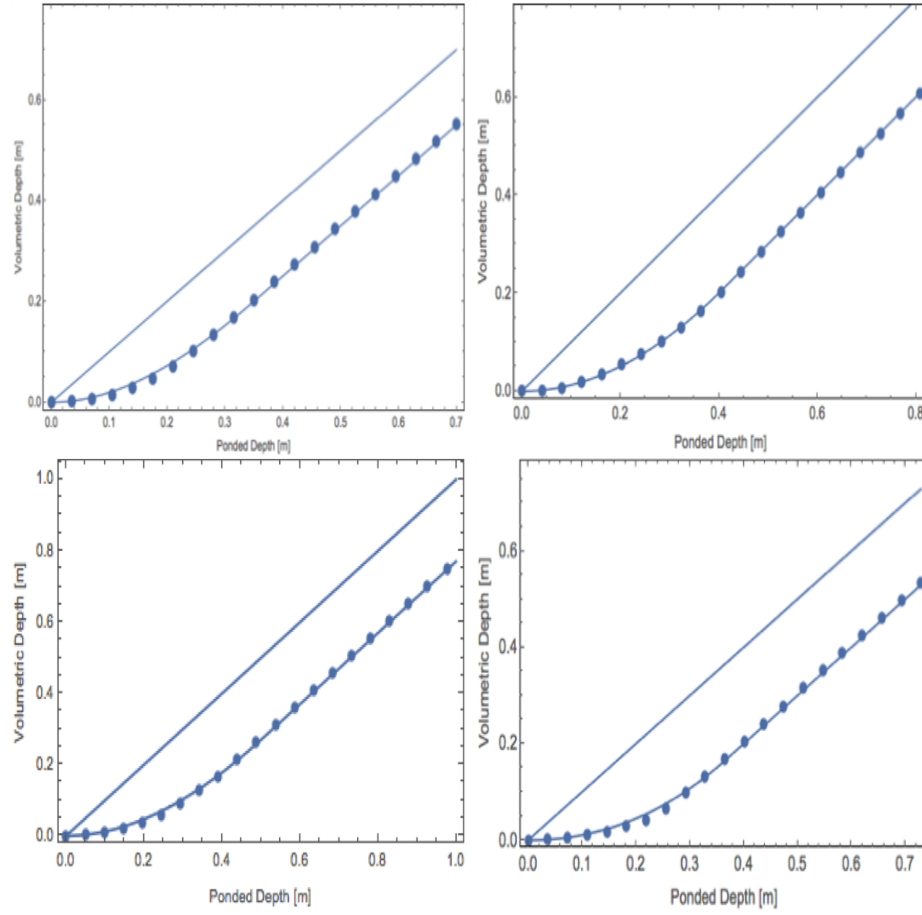


Figure 2: Volumetric depth versus pondered depth for four ice-wedge polygons. The ice-wedge polygons are displayed in Figure 4.

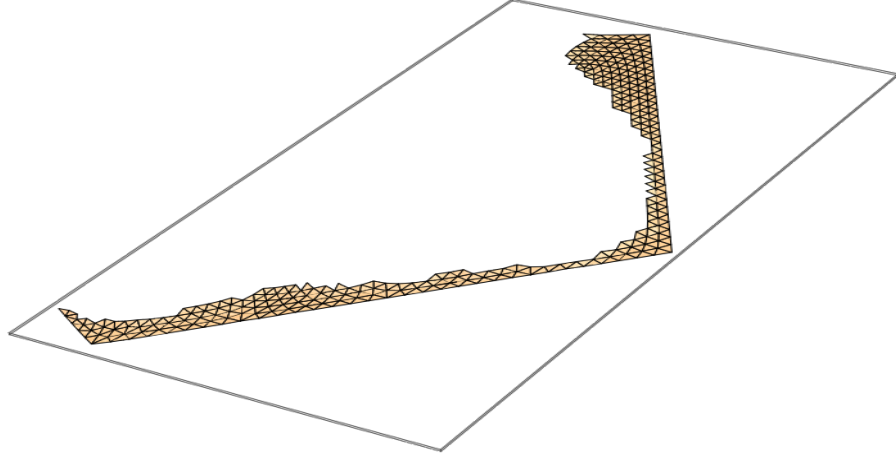


Figure 3: The spanning cluster at the percolation threshold for the IWP of Figure ?? . The water depth relative to the low point of the microtopography at the percolation threshold defines the depression depth.

- Specific excluded volume δ_{ex} , the soil volume above the microtopographic low point normalized by IWP area.
- Depression depth δ , the difference between the maximum and minimum elevation of the cells in the spanning cluster at the percolation threshold.

120

The subgrid releif and specific excluded volume come directly from the microtopography (univariate statistics). The depression depth requires a simple percolation algorithm to identify the spanning cluster at the percolation threshold. Values are given in Table 1.

125

Table 1: Parameters used in the subgrid model

	C06	C31	C40	C44	C45	A0	B01
$\delta_{\max}(m)$	0.404	0.262	0.483	0.364	0.350	0.361	0.411
$\delta_{\text{ex}}(m)$	0.2	0.105	0.23	0.2	0.15	0.185	0.26
$\delta_{\text{d}}(m)$	0.069	0.128	0.043	0.187	0.164	0.222	0.143

3. The Advanced Terrestrial Simulator (ATS)

Here we provide a very brief overview of the ATS for a reference, for more details about the software infrastructure we refer the reader to [20, 21].

130 A fully integrated surface/subsurface and snow distribution modeling capability implemented in ATS are available here [17, 22]. In addition, a mixed-dimensional modeling strategy, mainly designed for the simulations of low-relief permafrost-affected regions, can be found here [14]. The ATS is a publically-available massively parallel computer code, an extended ver-

135 sion of Amanzi (flow and reactive transport simulator; see [23]), based on process management tool called Arcos. In ATS, a proces kernel (PK) refers to governing mathematical equations representing a particular (or coupled) physical process(es). Further, Multiprocess Coordinators (MPCs) are available to facilitate coupling among PKs. The framework allows to dynam-

140 ically build a complex/coupled hierarchical model structure. The flexible extensibility feature of the Arcos framework allowed to easily implement our subgrid model and couple with the existing PKs.

4. Numerical Results and Discussions

4.1. Simulations

145 To assess the accuracy of numerical results of our subgrid model, we compare our results with fine-scale simulations and a coarsened model without subgrid (hereinafter referred to as “no subgrid model”). For demonstration purpose, the comparison is made for surface-only flow simulations. In our work, the seven ice-wedge polygons for fine-scale simulations are considered
150 from Barrow Environmental Observatory (BEO) and illustrated in Figure 4. The ice-wedge polygons named A, B and C correspond to the NGEE Arctic field sites A, B and C (see Figure 1), respectively. Those polygons consist of low-centered, high-centered, with well established troughs (relatively uniform elevation across the trough) and obstructions in the troughs, and hence
155 represent a broader class of polygonal landscape. Three sets of numerical experiments are performed with the subgrid model:

Study I: Evaluate the subgrid model with the parameters (uncalibrated) computed directly from surface microtopography;

Study II: Evaluate the subgrid model with calibrated values of the depression depth;
160

Study III: Evaluate the subgrid model with calibrated values of the depression depth and a drag coefficient. This is Study II with the inclusion of a drag factor in the flow law.

Study II is motivated by fine-scale simulations, higher depression depth
165 may delay breakthrough, and would lead to more accumulation of water in the depressions. That said, in Study II we adjust the value the depression depth computed by the percolation algorithm to provide a better fit to the

fine-scale results. The process of adjusting model’s parameters to replicate the benchmark (e.g., fine-scale computational or real experiments) results is known as calibration. Moreover, higher pressure in the subgrid model affects the overland conductivity and hence the discharge rate. To mimic the behavior of the fine-scale at the time of breakthrough and recession period, the surface roughness is decreased by raising the manning coefficient in the governing equation. This analysis proposed Study III. Raising the manning coefficient is analogous to introducing a drag factor.

A pulse numerical test (injection followed by recession) is performed in the above mentioned three numerical studies. That is, we start with a fully dry surface, and inject water at a constant rate at the inlet boundary until breakthrough happens (prescribed flux boundary for a certain period of time), then stop the water supply and let water pass through the outlet (free drainage boundary). The inward and outward arrows shown in Figure 4 indicate the inlet and outlet boundaries. To point out, the entire fine-scale IWP is considered as one coarsened grid cell in the subgrid and no subgrid model – the elevation of faces depends on the elevation of the corners of the fine-scale IWP. It is important to mention that the higher (inlet) and lower (outlet) boundaries are chosen based on the average elevation of the faces in the coarsened grid. For instance, the inlet_2 in the coarsened grid of the polygon A01 (shown in Figure 4) is higher than the outlet_2 , however, the fine-scale shows inlet_2 is lower than outlet_2 .

The rainfall events are not considered in Studies I, II and III. The presence of a fixed depression depth parameter in the flow law of our subgrid model will not allow to replicate the shape of the hydrograph because the fine-scale simulations will show immediate breakthrough. To capture such a behavior it would be more practical to determine the value of the depres-

195 sion depth dynamicly – change the depression depth as the ponded depth
changes. This sort of research will be reported somewhere else.

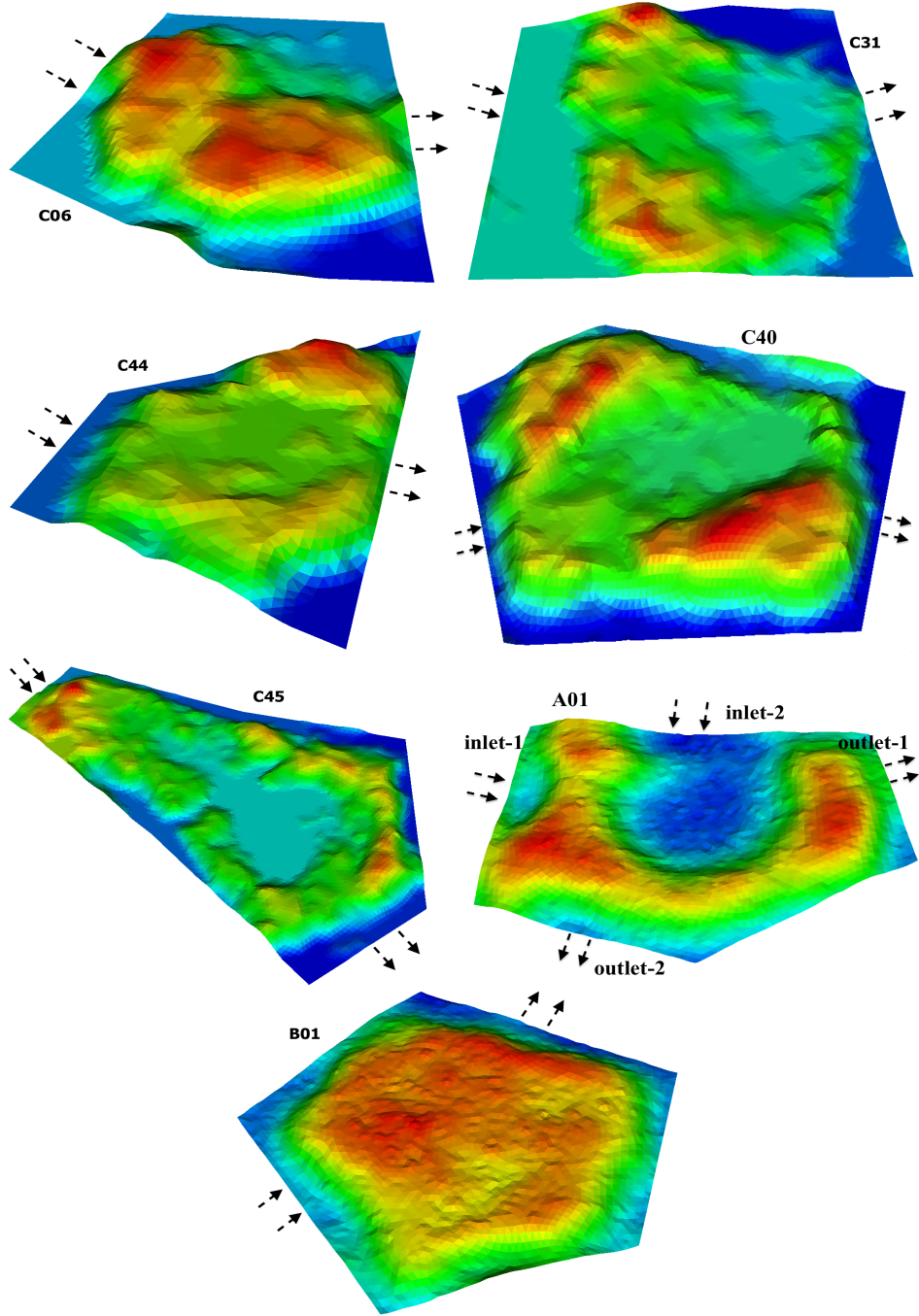


Figure 4: An Illustration of the microtopography of ice-wedge polygons from Barrow Environmental Observatory (BEO). Red and dark blue spots correspond to high- and low-elevated regions. The arrows indicate inlet and outlet boundaries.

4.2. Results and Discussions

Numerical results presented in this subsection correspond to the three studies mentioned above. We compare our results with fine-scale simulations of single IWPs, and we do not present any results on a cluster of fine-scale IWPs. We have carried out detailed simulations on all the polygons shown in Figure 4, however, we discuss the results of polygon C44 in more detail and these results serve as a representative of all the remaining polygons as far as the accuracy and shape of the hydrographs are concerned. Figure 5 compares the numerical results of the subgrid model with the fine-scale simulations, and no subgrid model of polygon C44. Clearly, Study I fails to match the fine-scale simulations, delayed breakthrough in the subgrid model is an indication of higher depression depth computed by the percolation algorithm; see Figure 5(a). Simulations with a calibrated depression depth, Study II, dramatically improve the shape of the hydrograph and the water content in the system as shown in see Figure 5(b). However, a mismatch appears at the time of breakthrough and the beginning of recession period even with the use of a calibrated depression depth. As alluded to earlier, this is due to the huge head gradient between the center and seepage face, and physically makes sense. Figure 5(c) illustrates the results of Study III, and it is evident that our subgrid model reproduces the fine-scale behavior, and the numerical results are identical to the fine-scale simulations. However, a complete mismatch is observed in numerical results of the no subgrid model.

Figure 6 compares the numerical results of Study I and III with the fine-scale and no subgrid model. The percolation algorithm computed the depression depth very accurately for polygon C06, and calibration (Study II) is not required. Similar to the results of polygon C44, the high over-land conductivity in the subgrid model is reduced by increasing the surface

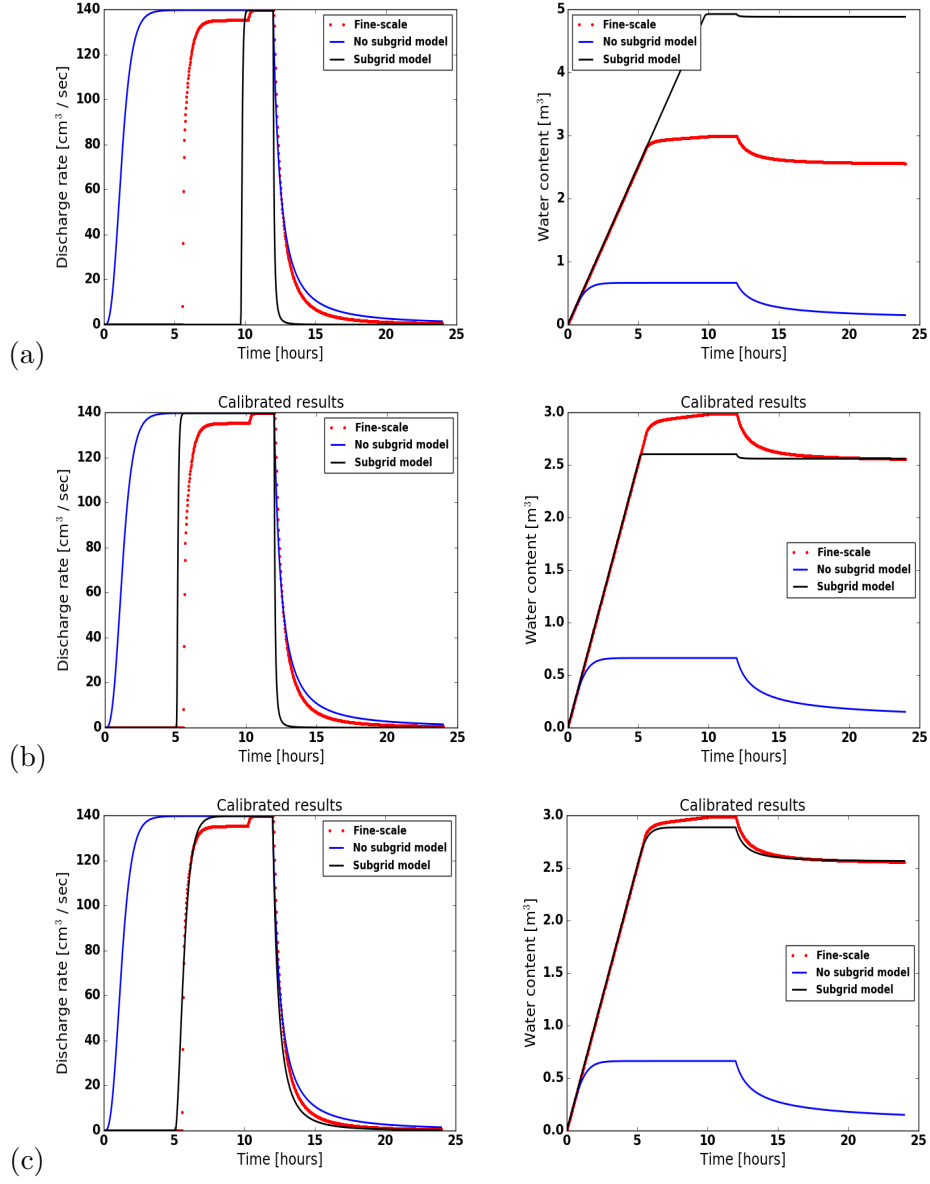


Figure 5: (Polygon C44) Comparison of the numerical results of the subgrid model with the fine-scale and no subgrid model results. Rows (top to bottom) correspond to Study I, II and III, respectively.

roughness. It improves the results and replicate the recession period of the
 225 fine-scale results. Figure 6 also displays the water retained in the subgrid
 and fine-scale models, the match is very close. For polygon C31, the results
 of the subgrid model are strongly affected by the depression depth in Study
 I, and lead to a mismatch. However, the results of Study II and III indicate
 that calibrated values of the depression depth and the surface roughness
 230 improved the simulated results dramatically and yield a close match as de-
 picted in Figure 7. Numerical simulations correspond to polygons C40, C45,
 A01, and B01 are shown in Figures 8, 9, 10, and 11, respectively. In Fig-
 ure 10, the results correspond to inlet₂ and outlet₂ boundaries, the results
 using inlet₁ and outlet₁ are discussed later in this subsection. Overall, the
 235 results of the subgrid model are very encouraging and consistently yield a
 better fit to the fine-scale results as compared to the no subgrid model.

4.3. Additional Remarks

- Not surprisingly, the subgrid model favors high surface roughness that
 swings the results toward fine-scale simulations. A high agreement
 240 between the results of the subgrid model and fine-scale simulations due
 to reduced runoff is an indication of a needed drag coefficient in the
 flow law. A linear regression fit to the drag factor vs. the depression
 depth is depicted in Figure 12. The drag factor varies between zero and
 one, as the depression depth decreases the drag factor goes to unity
 245 – a representation of flow over a flat surface. The fit indicates the
 resistance to flow increases with increasing depression. This finding is
 highly consistent with the discussion regarding the conductance terms
 in [19].
- For low-centered polygons such as C45 and A01, Study I (uncalibrated

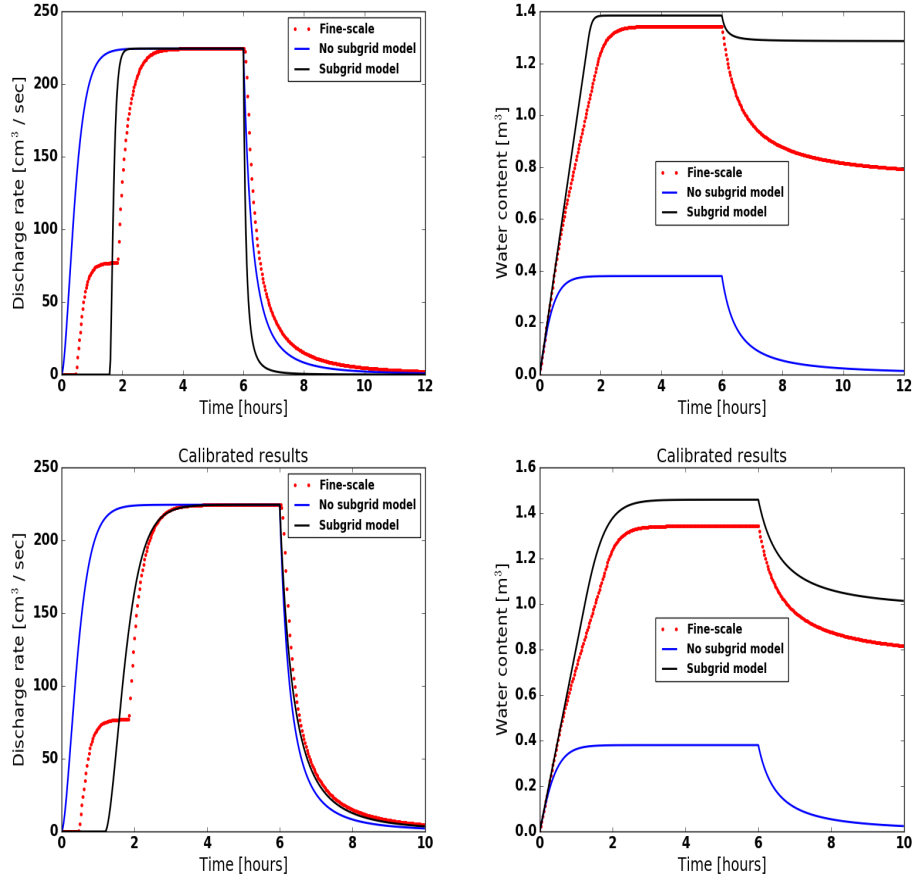


Figure 6: (Polygon C06) Comparison of the numerical results of the subgrid model with the fine-scale and without subgrid model results. Top and bottom row correspond to Study I and Study III, respectively.

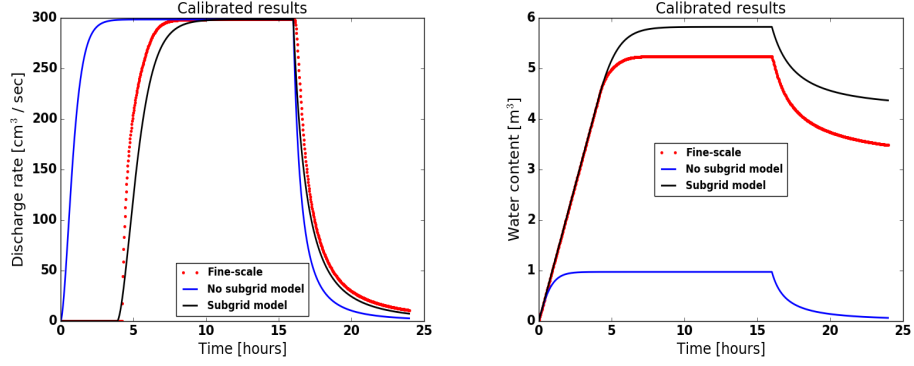


Figure 7: (Polygon C31) Comparison of the numerical results of the subgrid model with the fine-scale and no subgrid model. Results corresponded to Study III.

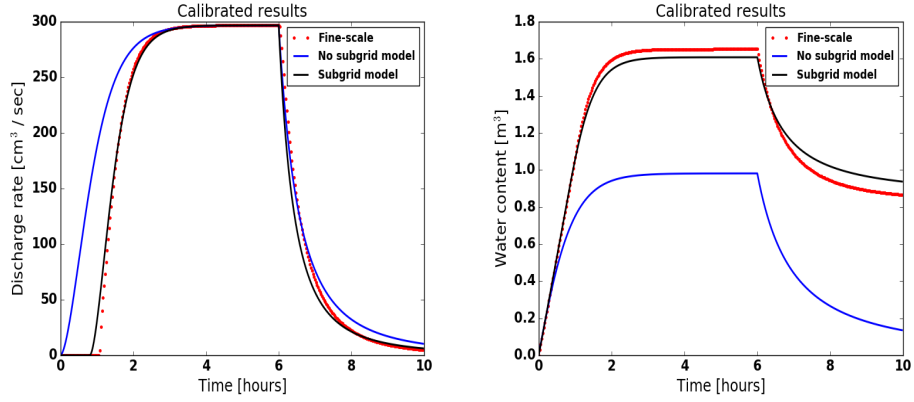


Figure 8: (Polygon C40) Comparison of the numerical results of the subgrid model with the fine-scale and without subgrid model results. Bottom row displays calibrated results.

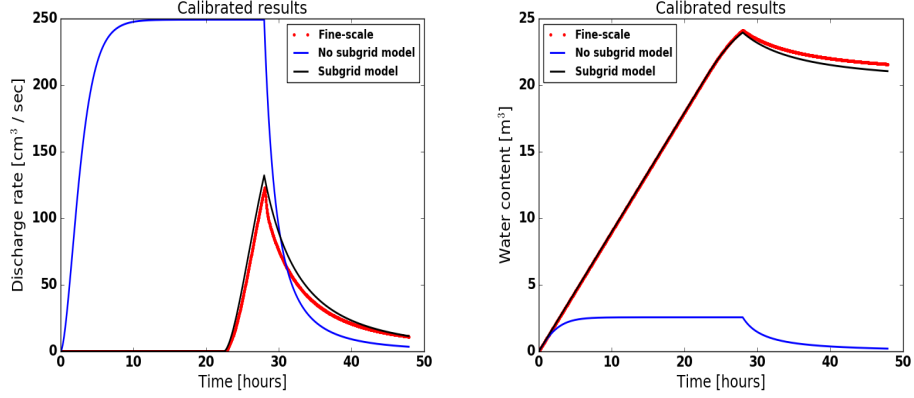


Figure 9: (Polygon C45) An illustration of the numerical results of the subgrid model, the fine-scale and no subgrid model. The simulations correspond to Study III.

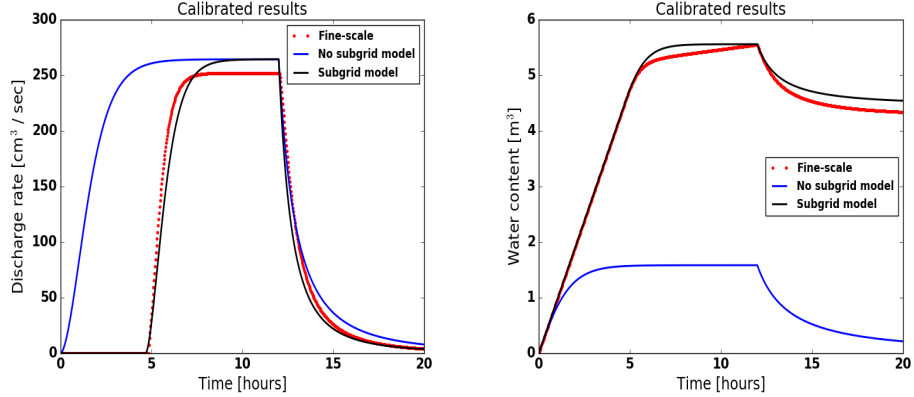


Figure 10: (Polygon A01) Comparison of the hydrographs and water content from the numerical simulation of the fine-scale, subgrid and no subgrid models. The results correspond to inlet₂ and outlet₂ boundaries.

250

results) fails to match the hydrograph of the fine-scale simulations – no breakthrough happens if uncalibrated depression depths are used. Fine-scale simulations show that low-elevated regions may remain completely dry if they are not located in the main flow channel which is trivial. However, as stated earlier, our percolation algorithm fills the

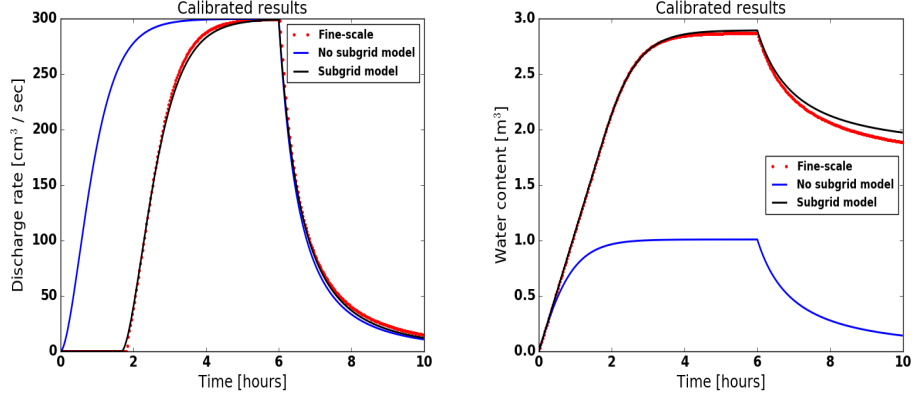


Figure 11: (Polygon B01) Comparison of the numerical results of the subgrid model with the fine-scale and without subgrid model results.

lowest elevation cells until the cluster of inundated cells spans the IWP. Thereby, the direction of the injected fluid is important. For instance, considering polygon A01, the results are not comparable if the inlet and outlet are at sides inlet_1 and outlet_1 , respectively. However, if the inlet and outlet are switched to inlet_2 and outlet_2 a desirable match is obtained; see Figure 13.

- An empirical relation correlating the uncalibrated (directly measured from the microtopographic data) and calibrated (insight from fine-scale simulations to adjust the uncalibrated values) depression depths is shown in Figure 12. The fitted curve with the coefficient of determination 0.82 yields a good match. As a subject for future research, the application of invaded percolation (flow in the direction of least resistance) algorithm could provide more accurate depression depths, and would probably overcome the issues of calibrating parameters and/or location of inlet and outlet boundaries.

- Most of our numerical experiments show that the subgrid model outperforms the no subgrid model even when the fine-scale flow behavior is not completely captured.
- When the inlet boundary has obstructions (for example, polygon C06 in Figure 4) and divides the incoming water into different flow channels, the water reaches the outlet boundary at different times and lead to a dual-peak (or may be multiple-peak) hydrograph. Due to only one grid cell in the subgrid model, the dual-peak behavior is not possible to capture.

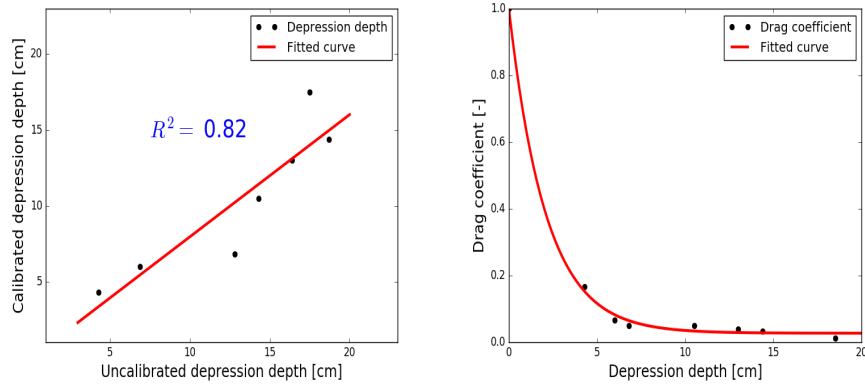


Figure 12: (Left) Linear fitted-curve to the depression depth data. (Right) Drag factor vs. calibrated depression depth.

5. Conclusions

The subgrid model presented in this paper is aimed at incorporating the microtopographic effects in the governing equations for the simulations of integrated surface/subsurface processes at watershed-scale.

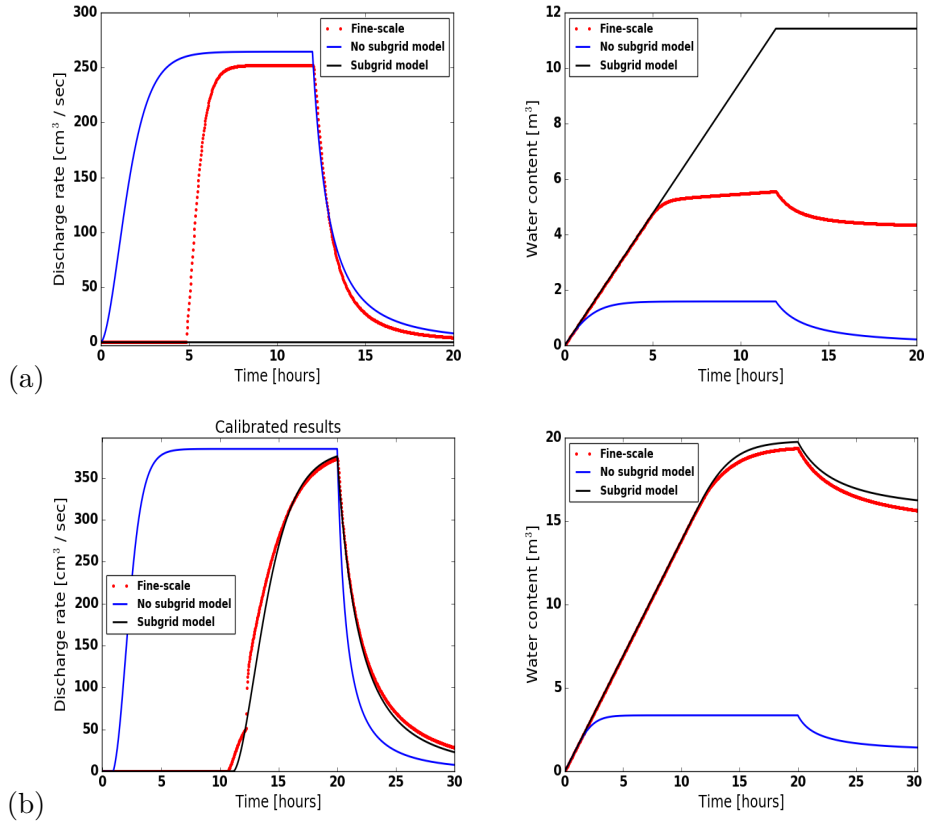


Figure 13: (Polygon A01) An illustration of the numerical results based on the choice of the inlet and outlet boundaries. The orientation affects the match between the fine-scale and subgrid model. (a) inlet₁ and outlet₁ boundary; (b) inlet₂ and outlet₂ boundary.

285

Standalone fine-scale surface simulations are tractable with the existing sophisticated computing tools. However, a significant challenge is how to capture accurate flow behavior in the watershed-scale integrated models because fine-scale simulations of integrated models at such a scale are not feasible. Seven fine-scale ice-wedge polygons are considered to demonstrate that the effect of surface microtopography can be captured in coarsened models through the use of a subgrid

290 model. Numerical results of the subgrid model compare very well
 with the fine-scale simulations. Our analysis shows that accurate es-
 timate of depression depth is a determining factor for a close match
 between subgrid and fine-scale simulations. Three different studies are
 conducted to estimate the parameters: (1) direct measurements from
 295 topography; (2) insight from fine-scale simulations to calibrate; (3) and
 empirical adjustment of topography-derived values. Thus the effort to
 obtain a reasonable match with the fine-scale simulations using coars-
 ened meshes with a subgrid representation was highly successful. The
 model is applied to 468 polygons watershed and a comparison is made
 300 no subgrid model. Numerical results demonstrate the importance of
 microtopography effects in watershed-scale simulations. **(this part
 will change once we add 486 polygons results)**. The subgrid
 model’s ability to accurately capture fine-scale flow behavior provides
 confidence that a few parameters extracted from the available micro-
 305 topographic data can be used to incorporate the fine-scale effects in
 watershed-scale integrated models. However, more research is needed
 to extend the approach developed here to accurately simulate problems
 involving both runoff and precipitation.

References

- 310 [1] E. A. G. Schuur, A. D. McGuire, C. Schaedel, G. Grosse, J. W.
 Harden, D. J. Hayes, G. Hugelius, C. D. Koven, P. Kuhry, D. M.
 Lawrence, S. M. Natali, D. Olefeldt, V. E. Romanovsky, K. Schae-
 fer, M. R. Turetsky, C. C. Treat, J. E. Vonk, Climate change and
 the permafrost carbon feedback, *NATURE* 520 (2015) 171–179.

- 315 [2] G. Hugelius, J. Strauss, S. Zubrzycki, J. W. Harden, E. A. G.
Schuur, C.-L. Ping, L. Schirrmeister, G. Grosse, G. J. Michaelson,
C. D. Koven, J. A. O'Donnell, B. Elberling, U. Mishra, P. Camill,
Z. Yu, J. Palmtag, P. Kuhry, Estimated stocks of circumpolar per-
mafrost carbon with quantified uncertainty ranges and identified
320 data gaps, *Biogeosciences* 11 (2014) 6573–6593.
- [3] L. D. Hinzman, N. D. Bettez, W. R. Bolton, F. S. Chapin, M. B.
Dyrurgerov, C. L. Fastie, B. Griffith, R. D. Hollister, A. Hope,
H. P. Huntington, et al., Evidence and implications of recent cli-
mate change in northern alaska and other arctic regions, *Climatic*
325 *Change* 72 (2005) 251–298.
- [4] A. H. Lachenbruch, Mechanics of thermal contraction cracks and
ice-wedge polygons in permafrost, *Geological Society of America*
Special Papers 70 (1962) 1–66.
- [5] G. W. Greene, Contraction theory of ice-wedge polygons: A qual-
330 itative discussion, 1963.
- [6] J. R. Mackay, Some observations on the growth and deformation
of epigenetic, syngenetic and anti-syngenetic ice wedges, *Per-
mafrost and Periglacial Processes* 1 (1990) 15–29.
- [7] J. Mackay, Thermally induced movements in ice-wedge polygons,
335 western arctic coast, *Geomorphology: Critical Concepts in Ge-
ography* 5 (2004) 477.
- [8] J. Kumar, N. Collier, G. Bisht, R. T. Mills, P. E. Thornton, C. M.
Iversen, V. Romanovsky, Modeling the spatiotemporal variability

- in subsurface thermal regimes across a low-relief polygonal tundra
 340 landscape, *The Cryosphere* 10 (2016) 2241–2274.
- [9] M. T. Jorgenson, Y. L. Shur, E. R. Pullman, Abrupt increase
 in permafrost degradation in arctic alaska, *Geophysical Research
 Letters* 33 (2006).
- [10] A. K. Liljedahl, J. Boike, R. P. Daanen, A. N. Fedorov, G. V.
 345 Frost, G. Grosse, L. D. Hinzman, Y. Iijima, J. C. Jorgenson,
 N. Matveyeva, et al., Pan-arctic ice-wedge degradation in warm-
 ing permafrost and its influence on tundra hydrology, *Nature
 Geoscience* (2016).
- [11] J. C. Rowland, C. E. Jones, G. Altmann, R. Bryan, B. T.
 350 Crosby, L. D. Hinzman, D. L. Kane, D. M. Lawrence, A. Man-
 cino, P. Marsh, J. P. McNamara, V. E. Romanvosky, H. Toniolo,
 B. J. Travis, E. Trochim, C. J. Wilson, G. L. Geernaert, Arctic
 landscapes in transition: Responses to thawing permafrost, *Eos,
 Transactions American Geophysical Union* 91 (2010) 229–230.
- [12] A. Liljedahl, L. Hinzman, J. Schulla, Ice-wedge polygon type
 355 controls low-gradient watershed-scale hydrology, in: *Proceedings
 of the Tenth International Conference on Permafrost*, volume 1,
 2012, pp. 231–236.
- [13] J.-K. Huang, K. T. Lee, Influences of spatially heterogeneous
 360 roughness on flow hydrographs, *Advances in water resources* 32
 (2009) 1580–1587.
- [14] A. Jan, E. T. Coon, P. S. L., R. Garimella, J. D. Moulton,

- 365 An intermediate-scale model for thermal hydrology in low-relief
permafrost-affected landscapes, Submitted to Computational
Geosciences (2016).
- [15] S. Painter, J. Moulton, C. Wilson, Modeling challenges for pre-
dicting hydrologic response to degrading permafrost, *Hydrogeol-
ogy Journal* (2013) 1–4.
- 370 [16] B. L. Kurylyk, K. T. MacQuarrie, J. M. McKenzie, Climate
change impacts on groundwater and soil temperatures in cold
and temperate regions: Implications, mathematical theory, and
emerging simulation tools, *Earth-Science Reviews* 138 (2014) 313–
334.
- 375 [17] S. L. Painter, E. T. Coon, A. L. Atchley, M. Berndt, R. Garimella,
J. D. Moulton, D. Svyatskiy, C. J. Wilson, Integrated sur-
face/subsurface permafrost thermal hydrology: Model formula-
tion and proof-of-concept simulations, *Water Resources Research*
52 (2016) 6062–6077.
- 380 [18] W. N. Stammers, H. Ayers, The effect of slope and microtopog-
raphy on depression storage and surface detention, publisher not
identified, 1956.
- [19] S. Panday, P. S. Huyakorn, A fully coupled physically-based
spatially-distributed model for evaluating surface/subsurface
flow, *Advances in water Resources* 27 (2004) 361–382.
- 385 [20] E. T. Coon, J. D. Moulton, S. L. Painter, Managing complexity

in simulations of land surface and near-surface processes, *Water Resources Research* 78 (2016) 134–149.

[21] E. T. Coon, *ATS: The Advanced Terrestrial Simulator*, 2016.
<http://github.com/amanzi/ats>.

390 [22] A. L. Atchley, S. L. Painter, D. R. Harp, E. T. Coon, C. J. Wilson,
A. K. Liljedahl, V. E. Romanovsky, Using field observations to
inform thermal hydrology models of permafrost dynamics with ats
(v0.83), *Geoscientific Model Development* 8 (2015) 2701–2722.

395 [23] J. D. Moulton, M. Berndt, R. Garimella, L. Prichett-Sheats,
G. Hammond, M. Day, J. Meza, High-level design of amanzi,
the multi-process high performance computing simulator, office
of environmental management, united states department of en-
ergy, washington dc (2012).